Geophysical Journal International

Geophys. J. Int. (2011) **186,** 963–970 doi: 10.1111/j.1365-246X.2011.05099.x

Fault-zone healing effectiveness and the structural evolution of strike-slip fault systems

Yaron Finzi[1,3], Elizabeth H. Hearn[1], Vladimir Lyakhovsky[2] and Lutz Gross[3]

[1] *Department of Earth & Ocean Sciences, University of British Columbia, Vancouver, BC* V6T 1Z4*, Canada. E-mail: y.finzi@uq.edu.au*
[2] *Geological Survey of Israel, Jerusalem* 95501*, Israel*
[3] *Earth System Science Computational Centre, School of Earth Sciences, The University of Queensland, St Lucia, QLD* 4072*, Australia*

Accepted 2011 June 2. Received 2011 May 26; in original form 2011 January 19

SUMMARY

Numerical simulations of long-term crustal deformation reveal the important role that damage healing (i.e. fault-zone strengthening) plays in the structural evolution of strike-slip fault systems. We explore the sensitivity of simulated fault zone structure and evolution patterns to reasonable variations in the healing-rate parameters in a continuum damage rheology model. Healing effectiveness, defined herein as a function of the healing rate parameters, describes the post-seismic healing process in terms of the characteristic inter-seismic damage level expected along fault segments in our simulations. Healing effectiveness is shown to control the spatial extent of damage zones and the long-term geometrical complexity of strike-slip fault systems in our 3-D simulations. Specifically, simulations with highly effective healing form interseismically shallow fault cores bracketed by wide zones of off-fault damage. Ineffective healing yields deeper fault cores that persist throughout the interseismic interval, and narrower zones of off-fault damage. Furthermore, highly effective healing leads to a rapid evolution of an initially segmented fault system to a simpler through-going fault, while ineffective healing along a segmented fault preserves complexities such as stepovers and fault jogs. Healing effectiveness and its role in fault evolution in our model may be generalized to describe how heat, fluid-flow and stress conditions (that contribute to fault-zone healing) affect fault-zone structure and fault system evolution patterns.

Keywords: Elasticity and anelasticity; Fault zone rheology; Dynamics and mechanics of faulting; Fractures and faults; Crustal structure.

1 INTRODUCTION

In a typical fault zone, the principal slip surface is often surrounded by breccia and embedded within a damage zone that consists of open and healed fractures, veins, and other secondary features. Nested zones with increasing damage are present: Shallow distributed damage may be found up to several kilometres from the fault cores of large strike-slip faults. Within about 1 km of the active fault core, a zone of more intense damage is present. This zone may produce local seismic anisotropy (e.g. Boness & Zoback 2004), concentrate coseismic strain (e.g. Fialko *et al*. 2002) and elevate seismic scattering (e.g. Revenaugh 2000; Peng & Ben-Zion 2006). Within this zone, there is a 10–100-m-wide zone of intense damage which can trap seismic waves (e.g. Li *et al*. 1994; Ben-Zion *et al*. 2003) and may appear at the surface as a belt of pulverized fault zone rocks (e.g. Dor *et al*. 2006, 2008). Fault stepovers, kinks and bends, which are characterized by secondary fractures at various scales play an important role in the long-term evolution of fault systems (e.g. Kim *et al*. 2004). Persisting rigidity loss and modification of the stress state at these localities can also affect rupture propagation, ground shaking and fluid flow patterns (e.g. Biegel *et al*. 2008; Micklethwaite & Cox 2006).

In this paper, we study fault zone structure and fault system evolution using damage rheology implemented in 3-D simulations of strike-slip faults. Our numerical framework consistently describes the entire seismic cycle including damage accumulation and strain localization leading to macroscopic failure and stress-drop, and post-failure healing which represents material strengthening due to processes such as cementation, mineralization and compaction. Our simulations show that the damage zone structure along faults, the temporal stability of geometrical complexities, and the evolution of fault systems are all strongly affected by the effectiveness of healing. Specifically, more effective healing yields strong fault zones (lower interseismic damage level) with wider but shallower damage zones and shorter lived fault complexities (e.g. stepovers) compared to damage zones that undergo limited healing. In the following section we briefly describe the damage rheology model and constraints on the healing rate parameters. In Section 3, we present how healing effectiveness controls simulated damage zone structure, fault complexity and fault system evolution.

2 DAMAGE RHEOLOGY, HEALING FORMULATION AND MODELLING APPROACH

Many current fault system studies employ numerical simulations in which brittle rock is modelled as a rigid elastic-plastic solid, and faults are prescribed surfaces governed by friction. The main shortcoming of this approach is that it ignores gradual pre-failure material weakening and post-failure strengthening, and it consists of non-evolving faults and fault-zone material properties. While several recent studies simulate inelastic off-fault yielding as plastic strain (e.g. Andrews 2005; Ma 2008), the full simulation of fault-system evolution and related deformation fields requires concepts such as damage rheology that accounts for evolving elastic properties, off-fault deformation and spontaneous formation of new fault surfaces.

2.1 Damage rheology: theory

The damage rheology model we use (Lyakhovsky *et al*. 1997a,b) relates the elastic moduli to a single scalar variable (α) which reflects strength degradation due to crack formation and opening, with $\alpha = 0$ indicating undamaged rock and $\alpha = 1$ corresponding to a complete strength loss. Our rheology model, briefly described below, is fully described in previous publications (Lyakhovsky *et al*. 1997a,b; Hamiel *et al*. 2004; Ben-Zion & Lyakhovsky 2006).

To account for the evolution of material properties, the damage rheology model introduces a third elastic modulus (γ) and makes the elastic rigidity (μ) a function of the damage state variable, as follows:

$$\begin{aligned} &\lambda = \lambda_0 = \text{constant};\\ &\mu = \mu_0 + \gamma(\xi_0 - 0.5\xi) \approx \mu_0(1-\alpha);\\ &\gamma = \alpha\gamma_m; \end{aligned} \tag{1}$$

where λ and μ are the Lamé parameters of linear Hookean elasticity, and $\xi = I_1/\sqrt{I_2}$ is the strain invariants ratio ($I_1 = \varepsilon_{kk}$ and $I_2 = \varepsilon_{ij}\varepsilon_{ij}$ are the first and second invariants of the elastic strain tensor ε_{ij}). The parameter ξ_0 separates states of material degradation ($\xi > \xi_0$) and healing ($\xi < \xi_0$) associated with positive and negative damage evolution, respectively. Gamma (γ) is a damage related modulus required to describe strain energy of a damaged material (Lyakhovsky *et al*. 1997a,b). As damage accumulates (i.e. α increases), the rigidity (shear modulus μ) decreases and the damage related modulus γ increases from 0 (damage free) to its maximal value, γ_m, amplifying the non-linearity of rock elasticity.

At high confining pressure, low shear stress and high temperature, healing of microcracks is favoured, resulting in a recovery of elastic moduli. Our model healing formulation (eq. 2) is consistent with observations of a logarithmic increase of the friction coefficient with time (e.g. Dieterich 1978)

$$\frac{\mathrm{d}\alpha}{\mathrm{d}t} = C_1 \cdot \exp\left(\frac{\alpha}{C_2}\right) I_2\,(\xi - \xi_0) \qquad \text{for } \xi < \xi_0. \tag{2}$$

The healing rate (2) is a function of the material properties (C_1, C_2 and ξ_0), the state of the fault zone (α and I_2), and the ratio between confinement and shear (ξ). We note that temperature and fault-zone related heat evolution is not currently represented in our model. Assuming uniform initial damage levels and strain state (for example at a certain depth along a fully ruptured simple fault segment), the healing rate and damage level (during the healing stage) are primarily determined by the healing rate parameters C_1 and C_2. Depending on the combination of these parameters, the healing process may be slow or fast (post-seismically), and may yield insignificant or complete healing of the damaged material (Fig. S1).

As the healing process is typically fast and healing is only observed during the early post-seismic stage, parameters C_1 and C_2 can be used to estimate the near steady-state interseismic damage level along simple fault-segments (where strain state is uniform and stresses are dominated by healing and the regional stress field). Finzi *et al*. (2009) defined a characteristic interseismic damage level α_{ch} (termed the α_f in Finzi *et al*. 2009) which represents the estimated damage level after the healing rate reduces to a rate for which further detectable healing would occur on timescales comparable to a typical (moderate-large) earthquake cycle ($|\mathrm{d}\alpha/\mathrm{d}t| < 3 \times 10^{-11}\ \mathrm{s}^{-1}$, or $|\Delta\alpha| < 0.1$ in 100 yr). The characteristic damage level α_{ch} is calculated from eq. (2) assuming a strain invariant ratio suitable for healing ($\xi - \xi_0 \approx -1$), as follows:

$$\alpha_{ch} = C_2 \ln[3 \times 10^{-11}/C_1 I_2]. \tag{3}$$

While this threshold rate of $|\mathrm{d}\alpha/\mathrm{d}t| < 3 \times 10^{-11}\ \mathrm{s}^{-1}$ is arbitrary, applying a factor of 10 on the threshold rate would result in a very small change in the predicted damage level (α_{ch}). The magnitude of this change is $C_2 \cdot \ln(10)$ which for admissible values of C_2 ($C_2 < 0.04$; Finzi *et al*. 2009) is smaller than 0.1. The characteristic interseismic damage level α_{ch} also depends on the depth at which the healing occurs (through I_2 in eq. 3), and is therefore consistently calculated in this paper for a depth of 3–5 km. It is important to note that actual interseismic damage levels (in our numerical simulation and along natural fault zones), are expected to depart from α_{ch} values as a result of local variations in stress, in loading history and in fault geometry (Fig. S2).

Our analysis (Section 3) shows that variation of the healing parameters corresponding to variations in α_{ch} has an important effect on simulated damage-zone structure and fault-system evolution patterns. We therefore describe the healing process in terms of the overall effectiveness of healing (with $\alpha_{ch} > 0.65$ corresponding to ineffective or limited healing, and $\alpha_{ch} < 0.4$ corresponding to effective healing).

2.2 Up-to-date constraints on healing rate parameters

Due to a shortage of fault-damage observations at various stages of the earthquake cycle, previous attempts to constrain healing parameters have been primarily based on laboratory experiments and analytic considerations (e.g. Ben-Zion *et al*. 1999; Lyakhovsky *et al*. 2001). Finzi *et al*. (2009) further constrained the healing parameters based on estimates of fault-zone damage levels derived from trapped seismic wave and geodetic observations (Fialko *et al*. 2002; Peng *et al*. 2003; Li *et al*. 2006; Hamiel & Fialko 2007). The observations of rapid but incomplete healing along a variety of active faults supported using a range of healing parameters ($C_1 = 1 \times 10^{-24}$ to $1 \times 10^{-10}\ \mathrm{s}^{-1}$; $C_2 = 0.015$–0.035). The healing parameter space suggested by Finzi *et al*. (2009) is also supported by various studies suggesting that temporal changes in strong ground motion and wave propagation are related to fault-zone healing rates (e.g. Karabulut & Bouchon 2007; Wu *et al*. 2009; Zhao & Peng 2009). To update the constraints on healing parameters we use recent fault zone observations from the ECSZ (Cochran *et al*. 2009; Barbot *et al*. 2009; Hearn & Fialko 2009). These studies reveal a range of interseismic damage levels larger than that considered by Finzi *et al*. (2009) and they motivate us to use healing parameters that represent a larger range of α_{ch} values ($0.25 < \alpha_{ch} < 0.65$; Finzi *et al*.

2009 focused on a narrower range between 0.4 and 0.55). This wider range of admissible α_{ch} values is a more conservative assumption, given the uncertainties in estimates of interseismic damage levels and the uncertainty regarding the timing of observations within the earthquake cycle. Our current appreciation of the variability in interseismic damage levels enabled us to identify the previously underestimated effect that healing has on damage zone structure and evolution (fig. 8 in Finzi *et al*. 2009).

2.3 Modelling approach

We use 3-D realizations of a strike-slip fault system within a layered model governed by damage rheology. The model domain consists of a thin sedimentary layer underlain by visco-elastic layers representing the crust and upper mantle (assuming diabase and dunite flow laws with: pre-exponent $A = 6.3 \times 10^{-20}$ Pa^{-n}S^{-1}, power $n = 3.05$, activation energy $Q = 276$ kJ mol^{-1} and $A = 7.0 \times 10^{-14}$ Pa^{-n}S^{-1}, $n = 3.0$, $Q = 520$ kJ mol^{-1}, respectively; and a fixed geotherm of 20 °C km^{-1}). The modelled region is 100–250 km long (along strike), 100 km wide and 50 km deep (Finzi *et al*. 2009). For computational efficiency we suppress damage accumulation in the weak sedimentary layer (top 3 km of the model) by reducing the damage rate parameters to zero and fixing the damage level. Test models with damage not suppressed within the surface layer (not presented here) exhibit near-surface damage, which is somewhat wider, and more intense than our typical simulations. A variable force boundary condition (Lyakhovsky & Ben Zion 2008) is applied to the sides and bottom of the model domain, simulating a constant far field fault parallel velocity with relative rate of 32 mm yr^{-1} (corresponding to the San Andreas Fault). While our quasi-static model accounts for coseismic weakening and stress transfer, and it adequately reproduces earthquake scaling relations (Lyakhobsky & Ben-Zion 2008), the full effect of wave propagation and their interaction with damage are not simulated in our this work. More details of our typical model setup, layered earth model and parameters are given by Finzi *et al*. (2009).

3 RESULTS

3.1 Fault zone structure as a function of healing

Our simulations calculate the distribution of strain and damage within the model domain, from which we can calculate surface velocities, rigidity and other related quantities. Contiguous sets of elements that fail repeatedly, resulting in a higher damage level and lower rigidity than their surroundings, are interpreted as fault segments (fig. 4 in Finzi *et al*. 2009). Cross-sections through modelled fault segments (Fig. 1) display 'flower structures' with depth, which comprise of localized damage along the active fault core and a broader zone of distributed damage in the top 3–10 kilometres of the crust (Fig. 1). Finzi *et al*. (2009) showed that these flower structures are a robust feature persistent in all simulations with realistic crustal rheology and slip rate. The overall geometry of the 'flower-like' damage zones in our simulations is compatible with field observations (e.g. Sylvester 1988; Rockwell & Ben-Zion 2007; Zhao & Peng 2009) and with numerical simulations of off-fault deformation (e.g. Ma 2008). However, while such dynamic models with fixed material properties typically only describe coseismic damage patterns, our model accounts for damage processes occurring during many earthquake cycles (including all seismic-cycle stages) and they account for strain-localization feedback effects related to material evolution due to damage. Our model can therefore describe the inter-seismic evolution of the flower-like damage zone (Fig. 1), and can connect the inter-seismic structural properties of the fault-zone with long-term fault-system evolution (Section 3.2).

We define two damage subzones that are distinct in their evolution patterns, damage level, and spatial distribution. Localized Active Fault (LAF) damage represents the highly localized damage along the active fault cores (Fig. 1). LAF damage is coseismically very high, and it may rapidly heal at depth. Distributed Off-Fault (DOF) damage is the sustained, cumulative damage resulting from many earthquakes. The DOF damage develops

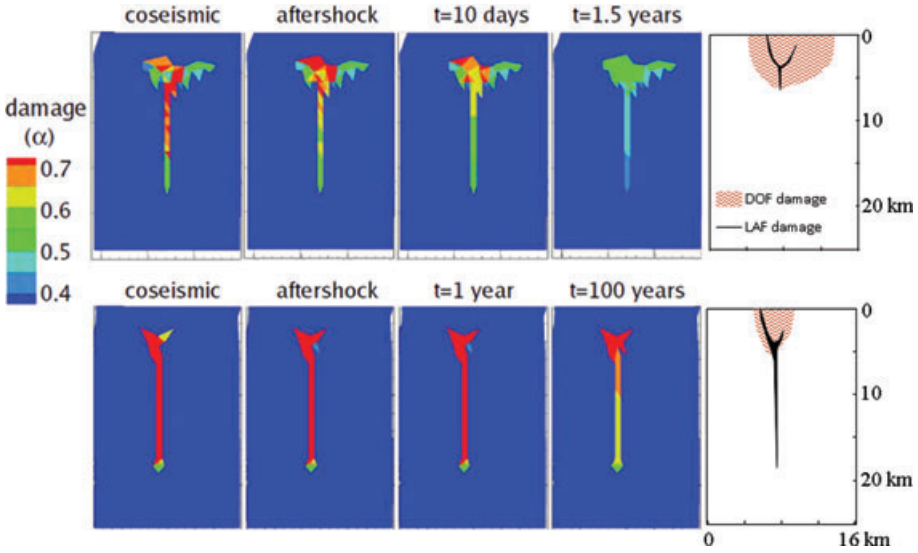

Figure 1. Schematic diagrams and cross-sections displaying evolving damage levels along two strike-slip faults representing effective (top, $\alpha_{ch} = 0.4$) and ineffective (bottom, $\alpha_{ch} = 0.7$) healing conditions. The schematic diagrams (top and bottom right panels) represent typical interseismic structures of distributed off-fault damage (DOF; red zones) and localized active-fault damage (LAF; black lines) in simulations with effective and ineffective healing. Shallow damage patterns ($z < 3$ km) presented in schematic diagrams were not simulated in these models, and are based on simple upward extrapolation of simulated damage patterns. All cross-sections are 25 km deep and 16 km wide.

during the early stages of fault system evolution, and thereafter its spatial extent is stable (Fig.1). Descriptive analyses of LAF and DOF damage structures along simulated strike-slip fault segments and along fault stepover zones are given in Finzi *et al*. (2009).

While our previous analysis concluded that the flower structure is a robust feature that shows limited sensitivity to variations in the healing parameters C_1 and C_2 (Finzi *et al*. 2009), we now realize that the effect of healing on damage zone structure is greatly enhanced when covarying both parameters to represent a wide range of α_{ch} values. Our results indicate that the depth extent of the LAF damage (after the early post-seismic interval) ranges from the entire seismogenic crust in fault zones experiencing ineffective healing ($\alpha_{ch} > 0.65$; Fig. 1 bottom panel; Fig. 2) to a few kilometres in fault zones experiencing effective healing ($\alpha_{ch} < 0.4$; Fig. 1 top panel; Fig. 2). Within the admissible parameter space for models of natural faults (i.e. for $0.25 < \alpha_{ch} < 0.65$), interseismic LAF damage along fault segments consists of intense and contiguous damage down to a depth of 5–15 km (Fig. 2). The dimensions of the shallow DOF damage are also sensitive to variations in the healing parameters. Simulations with ineffective healing result in faster (more complete) strain localization and therefore narrower fault zones, whereas simulations with effective healing exhibit migration of deformation and evolving fault configuration which yield wider fault zones (Figs 1 and 2).

It should be noted that our simulations probably overestimate the maximum width of fault damage zones as they do not incorporate depth-dependent damage-rate parameters, which would yield less damage accumulation in the top few kilometres of the crust (Lyakhovsky *et al*. 2005). In addition, our model element dimensions (1–3 km wide) may also contribute to an overestimated damage zone width, and they do not enable characterization of small-scale structures and extreme strain localizations along active slip zones.

3.2 Fault zone evolution patterns and temporal stability of fault stepovers

Strike-slip fault systems evolve over time. As total offset increases, frictional barriers to slip are reduced, segments lengthen and coalesce, and the fault straightens and simplifies. Detailed mapping of active and exhumed fault zones (e.g. Tchalenko 1970; Chester *et al*. 1993; Sibson 2003) indicate that the internal structure of fault zones evolves from distributed deformation through localization to principal slip zones, to mature large-scale faults with tabular damage zones and narrow cores of ultra-cataclasite (Lyakhovsky & Ben-Zion 2009). The slip rate along any new propagating fault by definition must experience a finite period of acceleration, and as it matures and the slip resistance decreases, the fault will accelerate to some steady-state slip rate.

Our previous simulations of damage zone evolution indicated that newly formed and propagating fault segments undergo a very short stage of complexity increase and DOF damage build-up (Finzi *et al*. 2009). During this early stage strain is distributed within widening damage zones, and fault segments interact to form damaged linking zones. We recently analysed the depth extent of the LAF damage and the slip-rate evolution as additional indicators of fault evolution. Our analysis indicates that the LAF damage reaches its maximum depth extent (i.e. coseismically reaches the bottom of the seismogenic zone) before the fault accumulate a large offset (offset < 0.5 km), with little sensitivity to the applied healing parameters. Similarly, the long-term (tectonic) slip-rate in our simulations is first achieved just before the fault DZ is fully established (after offset accumulation of the order of 0.1 km). While the fault damage-zone continues to form the fault experiences relatively small slip rate fluctuations around the tectonic slip-rate. After this, slip rate experiences sparse large fluctuations that slowly subside until the rate stabilizes at the long-term rate or until the system is perturbed by a change in regional stress or a dynamic change in fault configuration (Ando &

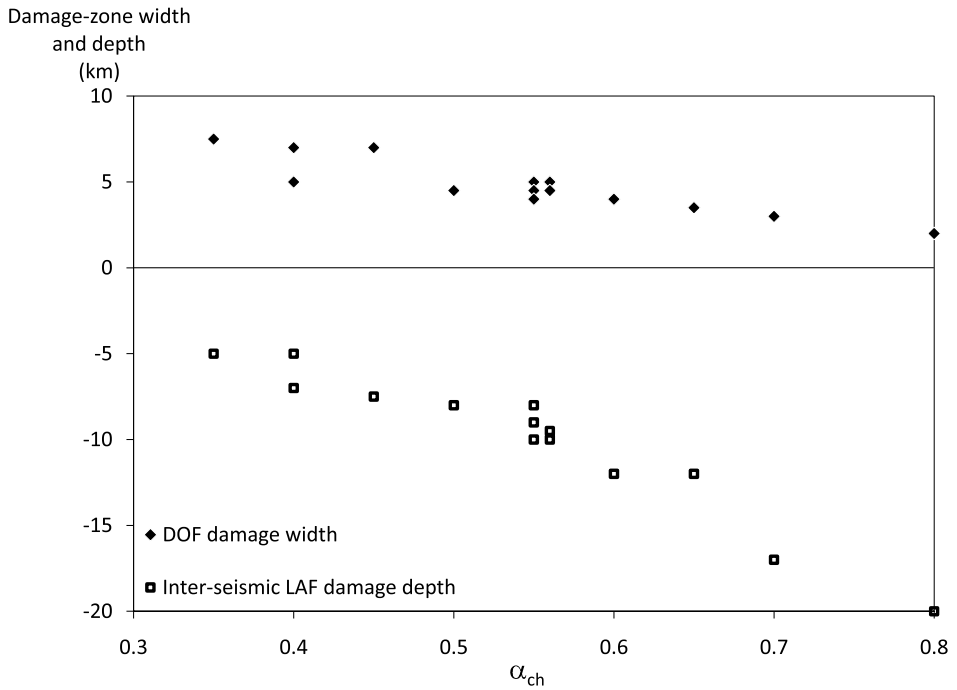

Figure 2. Sensitivity of damage zone dimensions to healing effectiveness. Simulations with ineffective healing (high α_{ch}) yield narrow DOF damage zones and interseismically deep LAF damage zones and simulations with effective healing yield wider and shallower damage zones. The width of distributed damage is measured at 5 km depth, and a damage level threshold of $\alpha > 0.5$ is used for measuring depth extent of the localized active-fault damage.

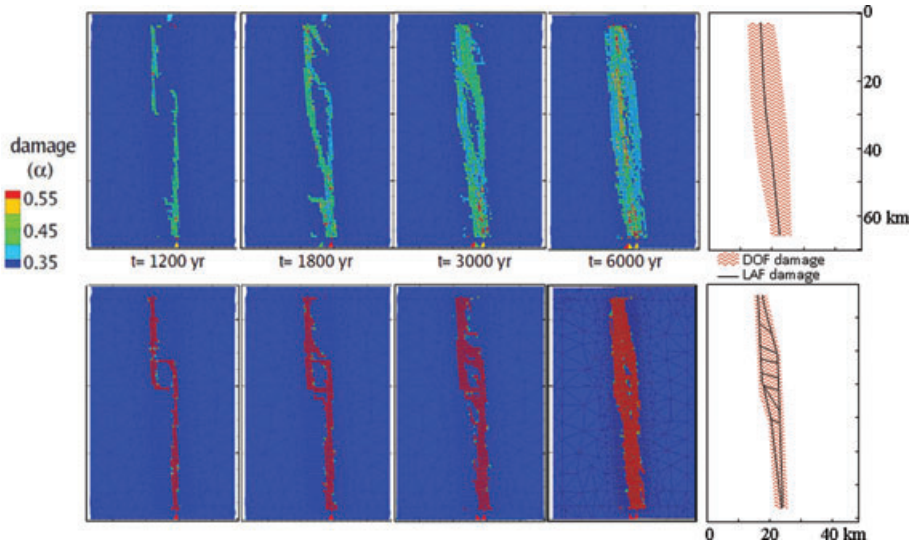

Figure 3. Damage maps and schematic diagrams displaying evolving stepover zones along two segmented strike-slip faults representing effective (top, $\alpha_{ch} = 0.4$) and ineffective (bottom, $\alpha_{ch} = 0.7$) healing conditions. While effective healing leads to rapid smoothing of the fault system and turns the stepover into an inactive structure traversed by a simple fault, ineffective healing keeps the stepover structure active and the fault system remains segmented throughout the duration of the simulation. All maps are 70 km long (along strike), 50 km wide and display damage at a depth of 5 km. The slip rate in presented simulations is 32 mm yr^{-1}. The schematic diagrams (right) represent fault configuration after thousands of years, black lines indicate active faults and red shading indicates damage at $z = 5$ km.

Yamashita 2007, Poliakov *et al*. 2002). The above perturbations of the fault maturation process (and their effect on damage zone structure) are not addressed in our this study. In our simulations, fault systems maintain a near tectonic slip rate only after deformation has localized along narrow slip-zones and after the faults are fully formed down to the bottom of the seismogenic zone (Fig. S3). While the healing parameters do not have a significant direct effect on the timescale of slip rate evolution in our simulations, the complexity of the fault system does affect the magnitude of slip rate fluctuations. In addition, simulations with effective healing are expected to evolve into simple fault systems and therefore should also yield relatively small slip rate fluctuations.

The short timescales for damage zone and slip rate maturation in the above simulations are generally consistent with various studies of exhumed fault zones (e.g. Chester *et al*. 1993; Evans *et al*. 2000), however, they do not incorporate the effect of large-scale persistent fault complexities that may impede localization. To study this effect we constructed a series of models simulating deformation patterns associated with a stepover zone between two en-echelon strike-slip fault segments. We focus these simulations on the evolution of dilatational (extensional) stepovers because they are a significant form of complexity, which spontaneously occurs in simulations applying fracture mechanics. The formation of such pull-apart stepovers is a natural outcome of the stress-field at a tip of a segment, which favours the nucleation of a second fault segment within the offset tensional-stress lobe. Other fault complexities (e.g. bends, gaps and compressional stepovers) would have internal structures and damage levels significantly different than those within tensional stepovers, however healing effectiveness would play a similar role in their temporal-stability. We find that these stepover zones may significantly slow down the process of complexity reduction and fault system maturation. In simulations with parameters that favour effective (near-complete) healing and yield low interseismic damage levels, fault stepovers evolve quickly into a single, contiguous fault segment that rapidly retains the characteristics of a mature fault segment (Fig. 3). In simulations with settings that favour ineffective (limited) healing, fault stepovers persist, slowing the simplification of the fault geometry (Fig. 3). As shown in Fig. 3, with effective healing the en-echelon faults link rapidly and the stepover is readily gapped changing the original structure to a through-going fault. At depth ($z > 5$–10 km; not shown in Fig. 3), the fault segments are rapidly and effectively healed and restrengthened in a way that they do not constitute a contiguous weak-zone and any subsequent earthquake would not necessarily re-rupture them. However, with very limited healing, stepovers and other fault complexities may grow with time but they are not expected to become inactive and give way to localized deformation on a through-going fault. This evolution pattern would yield long-lasting pull-apart basins or push-up swells with ongoing internal deformation, as is widely observed along segmented strike-slip faults. In addition, the depth extent of damage within stepover-zones is highly sensitive to healing effectiveness, with shallow stepover-damage (5–10 km deep) characterizing interseismic fault structures where conditions favour effective healing, and deep rooted stepovers (extending to a depth of 15–20 km) prevail where healing is ineffective (see also fig. 11 in Finzi *et al*. 2009). The limited depth extent of stepover-damage in simulations with effective healing may be interpreted as inactivation of the restrengthened fault segments at depth (below the shallow stepover zone). This interpretation provides a possible explanation for the observed rapid evolution of simulated en-echelon faults to a smooth continuous fault (in simulations with effective healing).

4 DISCUSSION AND CONCLUSIONS

Using a numerical model implementing damage rheology, an analysis of healing parameters and fault-zone geophysical observations, we have evaluated how material healing affects fault zone complexity, damage zone structure and long-term fault system evolution. Ben-Zion *et al*. (1999) and Lyakhovsky *et al*. (2001) previously analysed seismicity patterns along evolving strike-slip faults

in simulations with a narrow range of α_{ch} ($0.5 < \alpha_{ch} < 0.6$) and significantly different healing rates. They suggested that the ratio between healing and loading timescales controls fault zone complexity, where relatively fast healing and slow loading results in a disordered fault system. Their conclusion conforms with observations of repeating small ($M \sim 1.5$) earthquakes (with recurrence intervals of 3–600 d) for which the loading timescale is comparable to the healing timescale and loading impedes healing during the early post-seismic stage (e.g. Vidale *et al*. 1994; Marone 1998). However as recurrence times of moderate to large earthquakes vary between several decades and centuries (Nishenko & Buland 1987; Thatcher 1989), and observations of fault healing suggest a timescale of weeks-years (e.g. Peng *et al*. 2003; Li *et al*. 2006; Karabulut & Bouchon 2007; Wu *et al*. 2009; Zhao & Peng 2009;) it is unlikely that loading impedes healing in these conditions. Obviously, A fault with extremely fast loading rate and extremely slow healing might not experience a healing-period long enough to reach it's characteristic damage level (α_{ch}). While these special conditions are not the focus of our this work, they are addressed in previous work (Lyakhovsky *et al*. 2001) and they may represent conditions in areas loaded by large earthquakes or earthquake sequences.

In our model, the non-linearity of the healing process (eq. 2) decouples the healing timescale from the effectiveness of healing and the related residual damage level. Integration of eq. (2) reveals that the healing timescale is a function of the ratio C_1/C_2 and the magnitude of damage is scaled solely by C_2 allowing for a range of damage magnitudes to result from various healing processes with similar timescales. Analytic derivation of a non-dimensional healing equation confirms that the healing process is not fully determined by two parameters such as the timescale and initial damage level (Appendix). In this study, we analyse the role of α_{ch} in simulations of fault-zones where healing is very rapid and an interseismic (steady-state) damage level is achieved well before ruptured fault segments are significantly loaded. Our results, based on fully 3-D simulations and a wide range of healing parameters, provide important new insight on the healing process. This study extends and completes previous analyses of Finzi *et al*. (2009) and Lyakhovsky *et al*. (2001), by demonstrating that co-varying both healing parameters (C_1 and C_2) to represent variations in the characteristic interseismic damage level α_{ch} profoundly affects the modelled damage zone structure and fault system evolution.

In our simulations, faults with effective healing (associated with low inter-seismic damage levels along fault segments) produces wide, shallow damage zones and rapidly supersede pre-existing stepovers, whereas ineffective healing (high residual damage levels) produces fault systems with narrow, deep damage zones, and long-lived extensively damaged stepovers. In the effective healing case, a stepover is permanently weak only in the top few kilometres, and deeper coseismic damage is rapidly and effectively healed. Such a stepover has only a minor influence on the propagation of large ruptures, which break through it, eventually allowing a through-going fault to form. Where healing is limited, extensively damaged stepovers are expected to impede the evolution of the fault system into a simple through-going fault. The damage evolution patterns in our simulated fault stepovers are consistent with structural evolution models for dilatational stepovers (De Paola *et al*. 2007), and with studies of permeability evolution patterns along segmented faults (Micklethwaite & Cox 2004; Sheldon & Micklethwaite 2007). Healing effectiveness has important implications for permeability evolution and deposition processes which are directly affected by structural properties of the fault zone. The effect healing processes have on localization of deformation should also be considered in studies of large-scale plate boundary evolution. Persisting conditions favouring ineffective healing could preserve weakened structures influencing intraplate strain distribution, and conditions favouring effective healing could yield optimally oriented mature fault-systems that could localize strain on the continent scale. Finally, as healing proves to be important in strain localization and fault-system evolution processes, its role in continental break-up and rifting processes should be further examined.

As healing effectiveness controls the structure and evolution patterns of both the fault zone and the fault system in our simulations, we suggest that observable structural characteristics may be used to evaluate fault zone properties and conditions, and also to evaluate temporal stability of fault configurations. However, a better understanding (and formulation) of healing effectiveness is required. While healing effectiveness is currently estimated from material properties and depth (eq. 3), it could be generalized to incorporate factors such as regional loading geometry, fluid content and temperature. An alternative approach to estimating healing effectiveness could involve the assessment of conditions in respect to various strengthening mechanisms such as fracture closure, grain rearrangement, compaction and pressure solution (e.g. Beeler & Hickman 2004; Yasuhara *et al*. 2005; Chester *et al*. 2007). In addition, dynamic weakening and strengthening and processes of dynamic formation of complexity (e.g. branching) should also be considered in future studies of evolving fault structure and fault-systems (Lyakhovsky *et al*., 2011).

While linking between observable fault structures, long-term deformation patterns, and healing processes require additional support from fault zone observations and further analyses, the following features of fault zone structure and evolution appear to be robust in our simulations and are well supported by fault-zone observations:

(1) Fault zone healing is very rapid with most of the healing occurring within hours to days after an earthquake. Inter-seismically, fault zones exhibit a wide range of quasi-steady-state damage levels, with α between 0.25 and 0.65 (i.e. a rigidity reduction of approximately 25–65 per cent). We use the characteristic inter-seismic damage level (α_{ch}) and the term healing effectiveness to reflect this observation.

(2) Healing effectiveness is an important factor in the evolution of fault damage zones. Conditions favouring complete healing yield wider DOF damage in the top few kilometres of the crust and shallower fault-core LAF damage, whereas conditions favouring ineffective (limited) healing yield narrower DOF damage and deeper LAF damage zones.

(3) Healing effectiveness is an important factor in the temporal stability of fault stepovers. Fault complexities such as stepover zones are expected to be shorter-lived if fault zone conditions favour more complete healing.

(4) Fault stepovers exhibit large volumes of damaged material and are particularly sensitive to healing conditions. Our healing analysis suggests two feasible end-members of stepover structures with long-lived extensively damaged stepovers where $\alpha_{ch} > 0.65$, and transient shallow stepovers where $\alpha_{ch} < 0.4$. Seismic and geodetic observations of fault-stepover damage could provide important input for future analysis of fault-zone processes and fault system evolution.

ACKNOWLEDGMENTS

We thank the editor Xiaofei Chen, and two unknown reviewers for constructive reviews. We thank Yehuda Ben-Zion for his support and

useful comments throughout the process of the research and preparation of this paper. The study was supported by the Southern California Earthquake Center (based on NSF Cooperative Agreement EAR-0106924 and USGS Cooperative Agreement 02HQAG0008) and the US–Israel Binational Science Foundation, Jerusalem Israel (2008248).

REFERENCES

Andrews, D.J., 2005. Rupture dynamics with energy loss outside the slip zone. *J. geophys. Res.,* **110,** B01307, doi:10.1029/2004JB003191.

Ando, R. & Yamashita, T., 2007. Effects of mesoscopic-scale fault structure on dynamic earthquake ruptures: dynamic formation of geometrical complexity of earthquake faults, *J. geophys. Res.,* **112,** B09303, doi:10.1029/2006JB004612.

Barbot, S., Fialko, Y. & Sandwell, D., 2009. Three-dimensional models of elasto-static deformation in heterogeneous media, with application to the Eastern California Shear Zone, *Geophys. J. Int.,* **179,** 500–520, doi:10.1111/j.1365–246X.2009.04194.x

Beeler, N.M. & Hickman, S.H., 2004. Stress-induced, time-dependent fracture closure at hydrothermal conditions, *J. geophys. Res.,* **109,** B02211, doi:10.1029/2002JB001782.

Ben-Zion, Y. & Lyakhovsky, V., 2006. Analysis of aftershocks in a lithospheric model with seismogenic zone governed by damage rheology, *Geophys. J. Int.,* **165,** 197–210.

Ben-Zion, Y. & Sammis, C., 2003. Characterization of fault zones, *Pure appl. Geophys.,* **160,** 677–715.

Ben-Zion, Y., Dahmen, K., Lyakhovsky, V., Ertas D. & Agnon, A., 1999. Self-driven mode switching of earthquake activity on a fault system, *Earth planet. Sci. Lett.,* **172**(1–2), 11–21.

Ben-Zion, Y., *et al*., 2003. A shallow fault zone structure illuminated by trapped waves in the Karadere-Duzce branch of the North Anatolian Fault, western Turkey, *Geophys. J. Int,* **152,** 699–717.

Biegel, R., Sammis, C. & Rosakis, A., 2008. An experimental study of the effect of off-fault damage on the velocity of a slip pulse, *J. geophys. Res.,* **113,** B04302, doi:10.1029/2007JB005234.

Boness, N.L. & Zoback, M.D., 2004. Stress-induced seismic velocity anisotropy and physical properties in the SAFOD Pilot Hole in Parkfield, CA, *Geophys. Res. Lett.,* **31,** L15S17, doi:10.1029/2004GL019020.

Chester, F.M., Evans, J.P. & Biegel, R.L., 1993. Internal structure and weakening mechanisms of the San Andreas Fault, *J. geophys. Res.* **98,** 771–786.

Chester, F.M., Chester, J.S, Kronenberg, A.K. & Hajash, A., 2007. Subcritical creep compaction of quartz sand at diagenetic conditions: effects of water and grain size, *J. geophys. Res.,* **112,** B06203, doi: 10.1029/2006JB004317.

Cochran, E.S., Li, Y.G., Shearer, P.M., Barbot, S., Fialko, Y. & Vidale, J.E., 2009. Seismic and geodetic evidence for extensive, long-lived fault damage zones, *Geology,* **37**(4), 315–318, doi:10.1130/G25306A.1.

De Paola, N., Holdsworth, R.E., Collettini, C., McCaffrey, K.J.W. & Barchi, M.R., 2007. The structural evolution of dilational step-overs in regional transtensional zones, in *Tectonics of Strike-Slip Restraining and Releasing Bends,* pp.433–445, eds Cunningham W.D., Mann, P., Geological Society, London. Special Publication **290**.

Dieterich, J.H., 1978. Time-dependent friction and the mechanics of stick-slip, *Pure appl. Geophys.* **116,** 790–805.

Dor, O., Ben-Zion, Y., Rockwell, T. & Brune, J., 2006. Pulverized rocks in the Mojave section of the San Andreas Fault Zone, *Earth planet. Sci. Lett.*, **245,** 642–654, doi:10.1016/j.epsl.2006.03.034.

Dor, O., Yildirim, C., Rockwell, T., Ben-Zion, Y., Emre, O., Sisk, M. & Duman, T., 2008. Geologic and geomorphologic asymmetry across the rupture zones of the 1943 and 1944 earthquakes on the North Anatolian Fault: possible signals for preferred earthquake propagation direction, *Geophys. J. Int.,* **173,** 483–504, doi:10.1111/j.1365–246X.2008.03709.x.

Evans, J.P., Shipton, Z.K., Pachell, M.A., Lim, S.J. & Robeson, K., 2000. The structure and composition of exhumed faults, and their implication for seismic processes, in *Proceedings of the 3rd Conference on Tectonic Problems of the San Andreas System,* Stanford University.

Fialko, Y., Sandwell, D., Agnew, D., Simons, M., Shearer, P. & Minster, B., 2002. Deformation on nearby faults induced by the 1999 Hector Mine earthquake, *Science,* **297,** 1858–1862.

Finzi Y., Hearn, E.H., Lyakhovsky, V. & Ben-Zion, Y., 2009. Structural properties and deformation patterns of evolving strike-slip faults: numerical simulations incorporating damage rheology, *Pure appl. Geophys*., **166**(10), 1537–1573, doi:10.1007/s00024-009-0522-1.

Hamiel, Y. & Fialko, Y., 2007. Structure and mechanical properties of faults in the North Anatolian Fault system from InSAR observations of coseismic deformation due to the 1999 Izmit (Turkey) earthquake, *J. geophys Res.,* **112,** B07412, doi:10.1029/2006JB004777.

Hamiel, Y., Liu, Y., Lyakhovsky, V., Ben-Zion, Y. & Lockner, D., 2004. A Visco-elastic damage model with applications to stable and unstable fracturing, *Geophys. J. Int.,* **159,** 1155–1165.

Hearn, E.H. & Fialko, Y., 2009. Coseismic deformation of Mojave compliant zones and crustal stresses, *J. geophys. Res.,* **114,** B04403, doi:10.1029/2008JB005901.

Karabulut, H. & Bouchon, M., 2007. Spatial variability and non-linearity of strong ground motion near a fault, *Geophys. J. Int.,* **170,** 1, 262–274.

Kim, Y.S., Peacock, D.C.P. & Sanderson, D.J., 2004. Fault damage zones, *J. Struct. Geol.,* **26**, 503–517.

Li, Y.-G., Aki, K., Adams, D., Hasemi, A. & Lee, W.H.K., 1994. Seismic guided waves trapped in the fault zone of the Landers, California earthquake of 1992, *J. geophys. Res.,* **99**(B6), 11 705–11 722.

Li, Y.-G., Chen, P., Cochran, E.S., Vidale, J.E. & Burdette, T., 2006. Seismic evidence for rock damage and healing on the San Andreas Fault associated with the 2004 M 6.0 Parkfield Earthquake, *Bull. seism. Soc. Am.,* **96**(4B), S349–S363.

Lyakhovsky, V. & Ben-Zion, Y., 2008. Scaling relations of earthquakes and aseismic deformation in a damage rheology model, *Geophys. J. Int.,* **172,** 651–662, doi:10.1111/j.1365–246X.2007.03652.x.

Lyakhovsky, V., & Y. Ben-Zion., 2009. Evolving geometrical and material properties of fault zones in a damage rheology model, *Geochem*. *Geophys. Geosyst.,* **10,** Q11011, doi:10.1029/2009GC002543.

Lyakhovsky, V., Ben-Zion, Y. & Agnon, A., 1997a. Distributed damage, faulting, and friction, *J. geophys. Res.,* **102,** 27,635–27,649.

Lyakhovsky, V., Reches, Z., Weinberger, R. & Scott, T.E., 1997b. Non-linear elastic behavior of damaged rocks, *Geophys. J. Int.,* **130,** 157–166.

Lyakhovsky, V. Ben-Zion, Y. & Agnon, A., 2001. Earthquake cycle, faults, and seismicity patterns in rheologically layered lithosphere, *J. geophys. Res.,* **106,** 4103–4120.

Lyakhovsky, V., Ben-Zion, Y. & Agnon, A., 2005. A viscoelastic damage rheology and rate- and state-dependent friction, *Geophys. J. Int.,* **161,** 179–190.

Lyakhovsky, V., Hamiel, Y., & Ben-Zion, Y., 2011,. A nonlocal visco-elastic damage model and dynamic fracturing, *J. Mech. Phys. Solids,* doi:10.1016/j.jmps.2011.05.016, in press.

Ma, S., 2008. A physical model for widespread near-surface and fault zone damage induced by earthquakes, *Geochem. Geophys. Geosyst.,* **9,** Q11009, doi:10.1029/2008GC002231.

Marone, C., 1998. The effect of loading rate on static friction and the rate of fault healing during the earthquake cycle, *Nature,* **391,** 69–72.

Micklethwaite, S. & Cox, S.F., 2004. Fault-segment rupture, aftershock-zone fluid flow and mineralization, *Geology,* **32,** 813–816.

Micklethwaite, S. & Cox, S.F., 2006. Progressive fault triggering and fluid flow in aftershock domains: examples from mineralized Archaean fault systems, *Earth planet. Sci. Lett.,* **250**(1–2), 318–330.

Nishenko, S. P., & Buland, R., 1987. A generic recurrence interval distribution for earthquake forecasting, *Bull. seism. Soc. Am.,* **77**(4):1382–1399

Peng, Z. & Ben-Zion, Y., 2006. Temporal changes of shallow seismic velocity around the Karadere-Duzce branch of the north Anatolian fault and strong ground motion. *Pure appl*, *Geophys*. **163,** 567–600, doi:10.1007/s00024–005-0034–6.

Peng, Z., Ben-Zion, Y., Michael A.J. & Zhu, L., 2003. Quantitative analysis of seismic trapped waves in the rupture zone of the 1992 Landers, California earthquake: evidence for a shallow trapping structure, *Geophys. J. Int.,* **155,** 1021–1041.

Poliakov, A. N., Dmowska, B., R., & Rice, J. R., 2002. Dynamic shear rupture interactions with fault bends and off-axis secondary faulting, *J. geophys. Res.,* **107**(B11), 2295, doi:10.1029/2001JB000572.

Revenaugh, J., 2000. The relation of crustal scattering to seismicity in Southern California, *J. geophys. Res.,* **105,** 25 403–25 422.

Rockwell, T.K. & Ben-Zion Y., 2007. High localization of primary slip zones in large earthquakes from paleoseismic trenches: observations and implications for earthquake physics, *J. geophys. Res.,* **112,** B10304, doi:10.1029/2006JB004764.

Sheldon H. A. & Micklethwaite S., 2007. Damage and permeability around faults: implications for mineralization, *Geology,* **35**(10), 903–906.

Sibson, R.H., 2003. Thickness of the seismic slip zone, *Bull. seism. Soc. Am.* **93,** 3, 1169–1178.

Sylvester, A.G., 1988. Strike-slip faults, *Geol. Soc. Am.,* **100,** 1777–1703.

Tchalenko, J.S., 1970. Similarities between shear zones of different magnitudes, *Geol. Soc. Am. Bull.,* **81,** 1625–1640.

Thatcher, W. 1989. Earthquake recurrence and risk assessment in circum-Pacific seismic gaps, *Nature,* **341,** 432 − 434.

Vidale, J. E., Ellsworth, W., Cole, A. & Marone, C. 1994. Variations in rupture process with recurrence interval in a repeated small earthquake, *Nature,* **368,** 624–626.

Wu, C., Peng, Z. & Ben-Zion, Y., 2009. Non-linearity and temporal changes of fault zone site response associated with strong ground motion, *Geophys. J. Int.,* **176,** 265–278, doi:10.1111/j.1365–246X.2008.04005.x.

Yasuhara, H., Marone, C. & Elsworth, D., 2005. Fault zone restrengthening and frictional healing: the role of pressure solution, *J. geophys. Res.,* **110,** B06310, doi:10.1029/2004JB003327.

Zhao, P. & Peng, Z., 2009. Depth extent of damage zones around the central Calaveras fault from waveform analysis of repeating earthquakes, *Geophys. J. Int.,* **179,** 1817–1830, doi:10.1111/j.1365–246X.2009.04385.x

APPENDIX: NON-DIMENSIONAL HEALING EQUATION

To better understand the healing process and the non-unique relation between healing timescale and damage level we derive a non-dimensional form of the healing equation (eq. 2). Equation set (A1) states the general form of the healing equation and the scaling used for time and damage level

$$\begin{aligned} &\frac{\mathrm{d}\alpha}{\mathrm{d}t} = -A\mathrm{e}^{B\alpha} \\ &\alpha = \alpha_0\hat{\alpha} \qquad \text{with} \quad 0 \le \hat{\alpha} \le 1. \\ &t = \frac{\alpha_0}{A}\hat{t} \end{aligned} \tag{A1}$$

Parameters A and B in eq. (A1) are functions of the healing parameters C_1 and C_2, respectively (eq. 2). The non-dimensional healing equation can then be written as follows:

$$\begin{aligned} \frac{\mathrm{d}\hat{\alpha}}{\mathrm{d}\hat{t}} &= \frac{1}{\alpha_0}\frac{\mathrm{d}\alpha}{\mathrm{d}t}\frac{\mathrm{d}t}{\mathrm{d}\hat{t}} = \frac{1}{\alpha_0}(-A\mathrm{e}^{B\alpha})\frac{\alpha_0}{A} \\ &= -\mathrm{e}^{B\alpha} = -\mathrm{e}^{B\alpha_0\hat{\alpha}} = -\mathrm{e}^{K\hat{\alpha}} \text{ with } K = B\alpha_0. \end{aligned} \tag{A2}$$

Eq. (A2) indicates that an initial damage level and a timescale for healing do not fully determinate the healing process as the healing rate remains a function of an additional parameter K. In a similar way, the damage level can be shown to be a function of parameter K in the integral form of the non-dimensional healing equation.

SUPPORTING INFORMATION

Additional Supporting Information may be found in the online version of this article:

Figure S1. Damage as a function of time (after failure) for various sets of parameters C_1 and C_2 (parameters listed from top to bottom are: $C_1 = 1 \times 10^{-11}\ \mathrm{s}^{-1}, C_2 = 0.065, \alpha_{\mathrm{ch}} \approx 0.77$; $C_1 = 1 \times 10^{-32}\ \mathrm{s}^{-1}$, $C_2 = 0.0125$, $\alpha_{\mathrm{ch}} \approx 0.77$; $C_1 = 1 \times 10^{-08}\ \mathrm{s}^{-1}$, $C_2 = 0.065$, $\alpha_{\mathrm{ch}} \approx 0.32$; $C_1 = 1 \times 10^{-19}\ \mathrm{s}^{-1}, C_2 = 0.01, \alpha_{\mathrm{ch}} \approx 0.32$). The characteristic interseismic damage level (α_{ch}) and therefore also healing effectiveness are independent of the healing timescale. The healing curves represent end-members of very fast and slow healing, respectively, with fault observations indicating healing timescales spanning between that represented by red curves and some intermediate values between the red and blue curves.

Figure S2. Interseismic damage levels observed at $z = 5$–10 km in various simulations compared to calculated characteristic interseismic damage levels (α_{ch}) for the same depth. While the 1:1 correlation demonstrates the validity of using α_{ch} as a first order predictor of interseismic damage level (and healing effectiveness), the large variations of observed damage level certify that strain history and stress state are not homogeneous along fault segments in our models and are not expected to be homogeneous in nature. Observed damage was sampled along major fault segments in various simulation outputs (prior to any visualization smoothing). This procedure is subjective as the observer determines where damage is tapered to the background level of $\alpha = 0.1$–0.2 (introducing a minimal damage cut-off), and as the timing within the irregular seismic cycles in our simulations is also unclear.

Figure S3. Slip-rate and damage zone evolution with time. Slip rate averaged over several earthquake cycles (red), geological (cumulative) slip rate since the formation of the fault system (green), DOF damage width (yellow) and LAF damage maximum (coseismic) depth extent (blue). The damage zone width and depth are normalized to their value at the end of the simulation to indicate progress towards structural maturity. These dimensions and the slip rate initially increase rapidly (in association with the first large earthquake), then the slip rate fluctuates around the tectonic rate eventually approaching the long-term geologic rate (32 mm yr^{-1}). The healing parameters in this simulation correspond to $\alpha_{\mathrm{ch}} = 0.5$.

Please note: Wiley-Blackwell are not responsible for the content or functionality of any supporting materials supplied by the authors. Any queries (other than missing material) should be directed to the corresponding author for the article.